JJEE

Volume 10 | Number 3 | September 2024 | Pages 484-499

Jordan Journal of Electrical Engineering

ISSN (print): 2409-9600, ISSN (online): 2409-9619

Homepage: jjee.ttu.edu.jo

Far-Field Localization for RIS Empowered Wireless Systems Leveraging Beamforming

Abdulrahaman Kh. Alhafid[1*], Y. E. Mohammed Ali[2], Sedki Younis[3]

[1] Electrical Engineering Department, College of Engineering, University of Mosul, Mosul, Iraq
E-mail: abdulrhman.alhafid@uomosul.edu.iq

[2] Computer and Communications Engineering Department, College of Engineering, Nawroz University, Duhok, Kurdistan Region, Iraq

[3] Computer and Information Engineering Department, College of Electronics Engineering, Ninevah University, Mosul, Iraq

Received: Nov 27, 2023 *Revised: Feb 03, 2024* *Accepted: Feb 15, 2024* *Available online: June 23, 2024*

***Abstract*—** Reconfigurable intelligent Surfaces (RISs) have lately received a lot of interest due to their capability of providing a smarter controlled radio environment. This paper investigates the use of RIS beamforming to attain user equipment (UE) localization in far-field propagation with two localization schemes in millimeter-wave (mmWave) with orthogonal frequency division multiplexing (OFDM) signaling. The first scheme adopts a single RIS that leverages the time of arrival (ToA) and angle of departure (AoD) measurements. For this model, the impact of various parameters on the localization accuracy are examined. In addition, the Cramer-Rao Lower Bound (CRLB) for the positioning, i.e., the position error bounds (PEB), is derived to be used as benchmark. Also, an efficient multi-RIS aided localization scheme is proposed, in which the use of only AoDs to estimate the UE position is shown to be possible, whereas this was challenging without using multi-RIS scenario. The main contribution of this paper is relieving the complexity of localization algorithm by eliminating the necessity of ToA estimation where consensus-based fusion of AoDs estimations is used. The estimation of AoD from the RIS to the UE is obtained by using the RIS as a beamformer to scan the working area with successive beams. The highest received signal at UE from a particular beam will determine the AoD. The performance of the two localization models - discussed in this paper - are evaluated via extensive numerical simulations. For the first model, the simulation results and PEB demonstrated that increasing the number of beams that swept the region of interest has a significant impact on the accuracy, while using RIS with a large number of elements demonstrated marginal influence on the localization accuracy for a large number of RIS elements. Furthermore, the results reveal that the localization accuracy of the proposed multi-RIS localization scheme outperforms the performance of the first model by increasing the number of RISs and the number of beams. In addition, the proposed scheme benefits from being computationally efficient due to the release of ToA estimation in the first model that requires the computation of inverse fast Fourier transform (IFFT) of the oversampled version of the received signal for a sufficient number of transmissions and fine-tuning using search optimization to attain accurate estimation.

***Keywords*—** Reconfigurable intelligent surface; Localization; Far-field propagation; Beamforming; Beam sweeping; Time of arrival; Millimeter wave.

1. INTRODUCTION

The advent of 5G technology has expanded the capabilities of radio localization and enabled its facilities in several applications beyond its previous limitation to emergency call localization [1-4]. This capability may be achieved by using one or more 5G features like wideband signals, high carrier frequencies, and massive MIMO antennas, which can improve the localization performance in 5G networks [5-7]. On the other hand, with all these features, specific points have been raised about some challenges that will face the communication

* Corresponding author

DOI: https://doi.org/ 10.5455/jjee.204-1701118386

systems to ensure the quality of services in the presence of multi-path and energy consumption [8]. This indicates that since localization uses a lot of energy, it will be less attractive in general and practical usage. Renewable energy and devices with efficient energy consumption may alleviate some restrictions, but they may come with more complexity and a high cost [9].

The Reconfigurable Intelligent Surface (RIS) is a promising technology for wireless communications that has been developed and is anticipated to be used in 6G. RISs can increase coverage, enhance channel conditions, and improve the controllability of the multi-path environment [10]. Additionally, RISs are thought to be cost-effective since they are made up of passive components and have deficient energy consumption so they will enable ubiquitous communication with high efficiency in both energy and spectrum [11-13].

A RIS is an array of passive reflecting components that may be reconfigured to individually change the phase of an incoming signal. This capability allows for the creation of a programmable smart radio environment [14, 15], and it offers a wide range of soft-controlled electromagnetic features (such as beamforming, filtering, and focusing reflections) [16]. In addition, RIS systems can offer a reasonable tradeoff between hardware requirements and signal processing complexity. Furthermore, it is confirmed that the RIS can improve the connection quality over the standard arrangement without the RIS [17].

Furthermore, it has been observed that RISs possess significant capabilities in strengthening the accuracy of localization besides their role in improving communication [18]. Recently, several studies have examined the significance of RIS in enhancing the precision of localization. In [11, 19, 20], the Cramer-Rao Bound (CRB) is used to analyze the performance of RIS aided localization considering different system parameters, hardware assumptions, and communication scenarios. Localization in the near field using large RIS with efficient tile selection algorithms is investigated in [21–24] taking advantage of the enriched radio measurements. The optimization of the RIS phase profile and beamforming design was the main focus to improve the accuracy of the positioning system such as [7].

The study in [25] focuses on modelling and analyzing angle estimation errors using two dimensional discrete Fourier Transform (DFT) angle estimation. The approach involves extracting probability density functions (PDF) to represent the errors where the PDF is obtained by considering the geometric relationship of AoAs. The complex PDF formulation for AoA estimation error is then simplified using the first-order linear approximation of triangle functions. In [26] multiple RISs with single RF chains are utilized for UE indoor positioning. The UE direction is predicted by estimating the AoA for each RIS RF using different phase profiles. Based on the least squares line intersection from each RIS, maximum likelihood (ML) placement estimate is employed.

The suggested positioning method's accuracy is shown via PEB. The UE's location is estimated using ToA and AoD in [27]. A hybrid RIS with an RF chain is needed to estimate the channel from the transmitter to the UE through the RIS. The ToA is estimated using the same method as this study and AoD using the ML optimization scheme, which is more computationally expensive than beam sweeping. While the author in [28] considered the phase profile design of a single RIS to sweep the beam across the region of interest with time of arrival (ToA) estimation and cooperative uplink communication to enhance the accuracy of the localization.

In this paper, two localization models are discussed. The first model incorporates the ToA and the angle of departure (AoD) estimations of a single RIS localization presented in [28].

While the second model, which is the proposed model, introduces a multi-RIS scenario to devise a localization approach using only AoD measurements from multi-RIS. The performance of localization schemes is thoroughly investigated via numerical simulation. The contribution of this paper can be summarized as,

- The effects of designing parameters on the localization performance are investigated for the single RIS localization model using ToA and AoD estimations.
- The Cramer-Rao Lower Bound (CRLB) for the positioning, which is the position error bounds (PEB), is derived in this paper to be a benchmark for the localization performance.
- A localization scheme is proposed in the second model which adopt the beam sweeping scheme to estimate the AoDs for multi RIS scenario while alleviating the complexity as ToA estimation is not required. Consequently, the UE position is estimated using a consensus-based fusion of the estimated position of AoDs intersection.

The remainder of this paper is organized as follows. In section 2, the models of system geometry, the RIS, the channel, and the OFDM based system are described. The RIS aided localization using beam sweeping with two models and the derivation of Fisher information (FIM) and CRLB of the localization are introduced in section 3. In sections 4, we present the simulated scenario and discuss the performance analysis of the two models. Section 5 contains the concluding remarks.

Notations: Boldface lowercase characters, such as a, are used to denote vectors, while boldface uppercase letters, such as A, are used to represent matrices. The expression A_(i,j) refers to the element at i^th row and j^th column in matrix A. Transpose operator is represented (A)^T. while diag(a) and vec(A) are the operators that refer to the creation of a diagonal matrix using a vector a, and the vectorization of a matrix A, respectively. $\| . \|$ calculates the norm of vectors.

2. SYSTEM AND SIGNAL MODEL

In this paper, the considered system includes a base station with a single antenna, user equipment (UE) with a single antenna, and a single RIS or multi-RIS. As shown in Fig. 1, according to a general coordinate system, the locations of the RIS and the BS are fixed, known and indicated by $\boldsymbol{p}_A$ and $\boldsymbol{p}_{R_i}$ respectively, and the location of the UE, which is to be estimated, is indicated by $\boldsymbol{p}_U$.

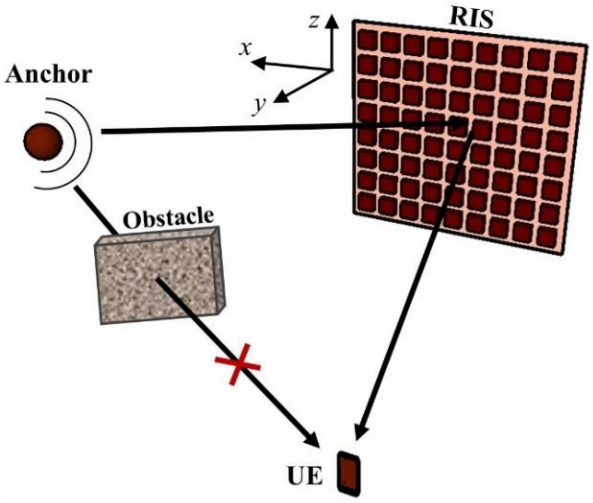

Fig. 1. The system and signal model.

The RIS consists of N_e elements arranged in uniform linear array (ULA) with $N_r \times N_c$ elements and inter-element distances equal to d_r and d_c respectively. So, the position of each element in each RIS coordinate system is denoted as $\boldsymbol{p}_e$ and expressed in $[x, y, z]$ coordinate as,

$$\boldsymbol{p}_e = \left[\left(n_c d_c - \frac{d_c(N_c-1)}{2}\right), 0, \left(n_r d_r - \frac{d_r(N_r-1)}{2}\right)\right] \quad (1)$$

where $n_c = 1,2, \ldots N_c$, and $n_r = 1,2, \ldots N_r$.

Each RIS element can be adjusted separately to vary the phase of the incident signal and reflect it. The same reflection coefficient is used for each column's elements for 2D beamforming.

The anchor transmits downlink orthogonal frequency division multiplexing (OFDM) signal for localization occasions. The OFDM signal has T pilot symbols, $t = 1, 2, \ldots T$, with N_{sc} subcarriers, $n = 1,2, \ldots N_{sc}$, the carrier frequency is centered at f_c and subcarriers spacing equal to Δ_f. By assuming that the direct line of sight (LoS) path between the anchor and the UE is obstructed by an obstacle, the signal will reach the UE via the virtual LoS path [29], i.e., through the RIS, which manipulates the incident signal according to a designed RIS phase profile. The amplitude and phase of the reflection coefficient for the n_e^{th} element of the RIS at each symbol transmission denoted as Υ and $\psi_{t,e}$, respectively. Then the reflection coefficient for each element will be,

$$w_{t,e} = \Upsilon\, e^{j\psi_{t,e}} \quad (2)$$

In other word, the RIS profile matrix at time t is $\boldsymbol{W}_t \in \mathbb{C}^{N_r \times N_c}$. The phase of the reflection coefficient $\psi_{t,e}$ is adjusted to have a value in the range of 0 to 2π, the adjustments could be made through a microcontroller connected to the RIS [30]. Also, a set of non-RIS NLoS paths may reach the UE. These non-RIS NLoS paths, whether formed by scatterers or reflectors, are often substantially weaker than the virtual LoS paths created by RISs. As a result, for notational simplicity, the non-RIS NLoS path will be excluded as in [29], and it will be taken into account through the additive noise in the received signal. Then, the received signal at the UE can be represented as,

$$\boldsymbol{Y} = x\, g_{ris}\, \boldsymbol{D}(\tau_{ris}) \odot \boldsymbol{A}(\Omega) + \boldsymbol{N} \quad (3)$$

where the received signal $\boldsymbol{Y}$ is a matrix of $\in \mathbb{C}^{N_{sc} \times T}$, $\boldsymbol{N}$ represents the noise matrix, each of its elements is randomly selected from a circularly symmetric Gaussian distribution with variance N_o including the impact of multi-path propagation in the environment, g_{ris} is the channel gain for the reflected path which can be described as [28, 31–33],

$$g_{ris} = \left(d_{A,ris}\, d_{ris,U}\right)^{-\frac{\mu}{2}} \quad (4)$$

where μ is the path loss exponent, $d_{A,ris}$ and $d_{ris,U}$ are the distances between the anchor and the RIS, and between the RIS and the UE, respectively, and x is the transmitted pilot symbols. For simplicity, it has been assumed that all the transmitted pilot symbols are equal to $x = \sqrt{E_s}$, with E_s being the energy of the symbol. The delay steering vector $\boldsymbol{d} \in \mathbb{C}^{N_{sc} \times 1}$ is repeated across time to be $\boldsymbol{D} \in \mathbb{C}^{N_{sc} \times T}$ which it is defined as,

$$\boldsymbol{D}(\tau_{ris}) = \boldsymbol{d}(\tau_{ris})\mathbf{1}_T^{\top} = \left[1, e^{-j2\pi\Delta_f \tau_{ris}}, \ldots, e^{-j2\pi(N_{sc}-1)\Delta_f \tau_{ris}}\right]^{\top} \mathbf{1}_T^{\top} \quad (5)$$

where Δ_f is the subcarriers spacing, τ_{ris} is used to account the propagation delay from anchor to UE through the RIS, i.e.,

$$\tau_{ris} = \frac{\|\boldsymbol{p}_R - \boldsymbol{p}_A\| + \|\boldsymbol{p}_U - \boldsymbol{p}_R\|}{c} \quad (6)$$

where c is the light speed. The parameter $\boldsymbol{A}(\Omega)$ in the received signal equation represents the compound steering vector for both incident steering vector $\boldsymbol{a}(\Omega_{in})$ and exit steering vector $\boldsymbol{a}(\Omega_{out})$ in addition to the RIS effect on the signal at time t. The RIS effect on the signal at time t is described by $\boldsymbol{W} \in \mathbb{C}^{N_e \times N_e}$ which is the diagonal matrix of the vectorized RIS phase profile $\boldsymbol{W}_t$, each entity on the diagonal is reflection coefficient of a RIS element,

$$\boldsymbol{W} = diag\big(vec(\boldsymbol{W}_t)\big) = diag\big(e^{j2\pi\theta_1}, e^{j2\pi\theta_2}, .., e^{j2\pi j2\pi\theta_{N_e}}\big) \tag{7}$$

So, as in [34] $\boldsymbol{A}(\Omega)$ can be written as,

$$\boldsymbol{A}(\Omega) = \boldsymbol{a}(\Omega_{in})^{\top} \boldsymbol{W}\, \boldsymbol{a}(\Omega_{out}) \tag{8}$$

where Ω_{in} is the known angle-of-arrival (AoA) from the anchor to the RIS, that is because both anchor and RIS positions are known, and Ω_{out} is the AoD from the RIS to the UE. Each AoA and AoD, in general, are composed of elevation (θ) and azimuth (φ) angles. The far field RIS steering vector $\boldsymbol{a}(\Omega) \in \mathbb{C}^{N_e}$ is defined as,

$$\boldsymbol{a}(\Omega)_e = \exp(-j\, \boldsymbol{k}(\theta, \varphi)^{\top} \boldsymbol{p}_e) \tag{9}$$

where $\boldsymbol{p}_e$ is the relative RIS element position and $\boldsymbol{k}(\theta, \varphi)$ is wavenumber vector which defined as [29],

$$\boldsymbol{k}(\theta, \varphi) = -\frac{2\pi}{\lambda} [\sin\theta \cos\varphi \quad \sin\theta \sin\varphi \quad \cos\theta] \tag{10}$$

where λ is the wavelength. Since the localization model is two-dimensional, then Ω_{in}, Ω_{out} and $\boldsymbol{k}$ will be described only by azimuth angle of the generic description above.

3. RIS AIDED LOCALIZATION USING BEAM SWEEPING IN THE FAR-FIELD

In this section, two models for UE localization are discussed. The first model, in subsection 3.1, follows a similar procedure presented in [28] of single RIS model which uses ToA and AoD. In the second model, subsection 3.2, the proposed multi-RIS aided localization scheme will be presented which use AoDs estimation for UE localization without the need of ToA estimation. In addition, the PEB is derived in subsection 3.3 to be used as a benchmark for positioning accuracy.

3.1. Model 1: Single RIS localization Model Using ToA and Beam Sweeping

The localization scenario in this model estimates the signal's ToA from the RIS to the UE and the signal's AoD from the RIS toward the UE and use them to estimate the location of the UE. The estimation of the ToA is achieved by exploiting the received OFDM signal in Eq. (3) and extract the estimated transmission delay $\hat{\tau}_{ris}$ as in [19]. The first step is to calculate the IFFT of the received signal as,

$$\boldsymbol{Y}_{IFFT} = IFFT(\boldsymbol{Y}) = \boldsymbol{F}\, \boldsymbol{Y} \tag{11}$$

where $\boldsymbol{F} \in \mathbb{C}^{N_F \times N_{sc}}$ is the IFFT matrix which has the elements as,

$$\boldsymbol{F}_{\boldsymbol{q},\boldsymbol{r}} = \frac{1}{N_F} e^{j2\pi qr/N_F} \tag{12}$$

$N_F = N_{os} N_{sc}$ determines the length of the IFFT vector, N_{os} is the IFFT oversampling factor. Hence, the OFDM symbol is divided to N_F parts and the ToA will be at the maximum value of the symbol, this maximum lies around (but not exact) some integer ℓ, where $\ell \in [0, N_F - 1]$, i.e.,

$$\bar{\tau}_{ris} = \frac{\ell}{N_F \Delta f} \tag{13}$$

To find the integer ℓ, the IFFT matrix is accumulated in time by taking the norm of each row, then performing an optimization search as,

$$\ell = \arg\max_{\mathrm{i}} \| \mathrm{e}_{\mathrm{i}}^{\top} \boldsymbol{Y}_{IFFT} \| \tag{14}$$

where $\mathrm{e}_{\mathrm{i}}^{\top} \boldsymbol{Y}_{IFFT}$ finds the i^{th}row in the IFFT of $\boldsymbol{Y}_{IFFT}$.

The estimation in Eq. (13) represents a coarse estimation of the ToA, and to refine this estimation, an artificial delay may be added to the integer ℓ, to satisfy the exact condition in Eq. (13). This can be achieved by adopting a quasi-Newton method using 0 as starting point, then,

$$\tilde{\delta} = \underset{\delta \in [0, 1/(N_F \Delta f)]}{\arg\max} \left\| \mathrm{e}_{\mathrm{i}}^{\top} \boldsymbol{F} \boldsymbol{Y}(\delta) \right\| \tag{15}$$

Finally, the accurate estimation of ToA will be,

$$\hat{\tau}_{ris} = \frac{\ell}{N_F \Delta f} - \tilde{\delta} \tag{16}$$

The estimated transmission delay $\hat{\tau}_{ris}$ converted to distance $\hat{d}_{ris}$ by multiplying it by the speed of light. This distance refers to the overall distance from the anchor to the UE through the RIS. Since the positions of the anchor and the RIS are known, then the estimated distance from the RIS to the UE $\hat{d}_{RU}$ could be found by subtracting the distance from anchor to the RIS from overall distance $\hat{d}_{ris}$.

Besides, the estimation of the AoD from the RIS to the UE is obtained following the considered framework in [28] using the RIS as beamformer to scan the working area with successive narrow beams, the highest received signal at UE from a particular beam will determine the direction of the UE i.e., the AoD. This method does not need any searching algorithm over the channel parameters and the observation signal which would be more complex than beam sweeping method. So, the estimation of the AoD using beam sweeping method requires a careful design of the RIS profile to perform this beam sweeping. Thus, to sweep the area of interest by S beams, it is necessary to design the RIS profile to have S configurations, each configuration will be applied to the RIS at a transmission t to direct a beam towards φ_s, where $\mathrm{s} \in (1, 2, .., S)$. To satisfy a beamforming towards φ_s, each row in the RIS profile $\boldsymbol{w}_{t,r} \in \mathbb{C}^{1 \times N_c}$ is configured as,

$$\boldsymbol{w}_{t,r} = \left(1, e^{j2\pi \frac{d_c}{\lambda} \varphi_{ris}}, .., e^{j2\pi \frac{d_c}{\lambda} (N_c - 1) \varphi_{ris}}\right) \tag{17}$$

The angle φ_{ris} should be described according to the received signal in Eq. (3) and its steering vectors in Eqs. (8) and (9). Since the localization model is two dimensional and the RIS is located at the (x, z) plane in the considered coordinate system, then the elevation angle will be 90^0 and the second and third term in the wavenumber vector in Eq. (10) will be eliminated. As a result, only the $cosine$ term will exist after multiplying the wavenumber vector by the position of the RIS element $\boldsymbol{p}_e$ in Eq. (9), then,

$$\varphi_{ris} = \cos(\varphi_i) - \cos(\varphi_r) \tag{18}$$

where φ_i is the known AoA from the anchor to the RIS, i.e., azimuth of Ω_{in}, φ_r is the desired sweeping angle, i.e., φ_s. To sweep an interested area confined between φ_1 and φ_2 with number of equally spaced beams S, the degrees for the angles of φ_s where $\mathrm{s} \in (1, 2, .., S)$ will be:

$$\varphi_s = \varphi_1 + \frac{(\varphi_2 - \varphi_1)}{S}(s - 0.5) \quad (19)$$

After this point, the UE determine the received signal level for each beam, the highest received signal power will determine the AoD for this UE, that is achieved by finding the index of the highest power beam as,

$$s_{max} = \underset{s\in(1,2,..,S)}{\arg\max} \| \boldsymbol{Y}_s \|^2 \quad (20)$$

The UE is assumed to lies at the center of the beam has the index s_{max}, i.e., the estimated AoD is $\varphi_{s_{max}}$. In this way, the amount of the received power has been utilized to estimate the UE direction with respect to the RIS. Then the estimated UE position is,

$$\hat{\boldsymbol{p}}_U = \left[x_{\mathrm{R}} + \hat{d}_{RU} \cos\varphi_{s_{max}} \ , \ y_{\mathrm{R}} + \hat{d}_{RU} \sin\varphi_{s_{max}}\right] \quad (21)$$

where x_{R} and y_{R} are the coordinates of the RIS, $\boldsymbol{p}_R = (x_{\mathrm{R}}, y_{\mathrm{R}})$

3.2. Model 2: Multi RIS localization Model Using Beam Sweeping

The localization scenario in this model uses number of RISs (N_{RIS}) with known positions, $\boldsymbol{p}_{R_i}$, i $\in (1, 2, .., N_{RIS})$ as shown in Fig. 2.

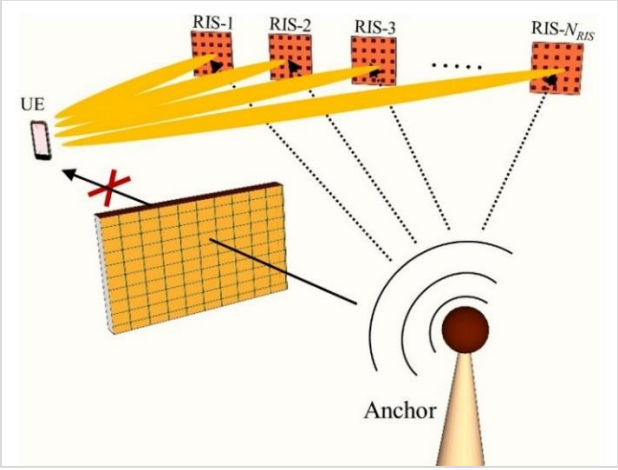

Fig. 2. Multi RIS localization Model.

By exploiting RIS beam sweeping method, which is described in section 3.1, the angle from each RIS towards the UE will be estimated. Each RIS performs a beam sweeping to scan the working area with S equally spaced beams. The working area is defined at each RIS by confining angles which select the start and end angles of the beam sweeping.

The highest received signal power from the RIS will determine the angle from that RIS towards the UE assumed the UE is lie at the center of the beam has the index of the maximum received signal as in Eq. (20). These AoD measurements from multiple RIS reference points are used to estimate the UE position. Algorithm 1 , describes the proposed localization method.

3.3. Fisher Information and Cramer-Rao Lower Bound

The Cramer-Rao Lower Bound (CRLB) is a fundamental concept in estimation theory that provides a lower bound on the variance of any unbiased estimator. In the context of UE location estimation, the CRLB can be used to assess the minimum achievable variance of an unbiased estimator for the location of a user [35]. In this section, the CRLB is evaluated for UE location estimation which uses ToA and AoD measurements to estimate the UE position [36].

Algorithm 1. Estimation of UE position using AoDs measurements

Input: Anchor position (p_A), RISs positions (p_{R_i}).

Initialize: number of beams (S), confining angles φ_1 and φ_2, RIS phase profile W.

for $n = 1$ to N_{RIS} do
  for $m = 1$ to S do
    Assign the particle RIS phase profile according to Eq. (17)
    Perform the beam sweeping
    Find s_{max} according to Eq. (20)
  end Estimate AoD, i.e., $\varphi_{s_{max}}$
end

Obtain: N_{RIS} of AoDs

for $i = 1$ to no. of AoDs do
  Find the line which the UE lies on it as, $y - p_{R_i,y} = \tan(\theta_{s_{max},i})\ (x - p_{R_i,x})$
end

Compute:

a. Intersection points for each two lines using trigonometric and vector methods

b. UE position from the intersection points using consensus fusion method

Output: The final estimation $\hat{p}_U$

The CRLB of an estimator can be obtained from the Fisher information matrix (FIM), which may be constructed using the log-likelihood function of the estimated parameters.

In this study, the estimator parameters vector can be written as,

$$\hat{\boldsymbol{a}}_{Est} = \left[\hat{\boldsymbol{d}}_{RU,i}^{\top}, \hat{\boldsymbol{\varphi}}_{RU,i}^{\top}\right]^{\top} \quad \in \mathbb{R}^{2N_{RIS}\times 1},\ i \in (1,2,..,N_{RIS}) \tag{22}$$

where $\hat{\boldsymbol{d}}_{RU,i}$ is the estimated distance, obtained from the estimated ToA, from the i^{th} RIS to the UE, and $\hat{\boldsymbol{\varphi}}_{RU,i}$ is the estimated azimuth angle between the i^{th} RIS to the US, i.e.,

$$\begin{aligned}\hat{\boldsymbol{d}}_{RU,i}^{\top} &= \left[\hat{d}_{RU,1}, \hat{d}_{RU,2} \dots \hat{d}_{RU,N_{RIS}}\right]\\ \hat{\boldsymbol{\varphi}}_{RU,i}^{\top} &= \left[\hat{\varphi}_{RU,1}, \hat{\varphi}_{RU,2} \dots \hat{\varphi}_{RU,N_{RIS}}\right]\end{aligned} \tag{23}$$

According to [36], the likelihood function of the estimator parameters vector $\hat{\boldsymbol{a}}_{Est}$, can be described as,

$$f(\hat{\boldsymbol{a}}_{Est}) = \prod_{i=1}^{N_{RIS}} \frac{1}{2\sqrt{2}\pi^3 \sigma_{d_{RU,i}} \sigma_{\varphi_{RU,i}}} e^{-\left[\frac{\left(\hat{d}_{RU,i}-d_{RU,i}\right)^2}{2\sigma^2_{d_{RU,i}}} + \frac{\left(\hat{\varphi}_{RU,i}-\varphi_{RU,i}\right)^2}{2\sigma^2_{\varphi_{RU,i}}}\right]} \tag{24}$$

Then, the CRLB of the estimator or the positioning error bound (PEB) can be written as,

$$PEB = \sqrt{Tr\left(\boldsymbol{FIM}_{\boldsymbol{p}_u}^{-1}\right)} \tag{25}$$

where $\boldsymbol{FIM}_{\boldsymbol{p}_u}^{-1}$ is the inverse of FIM for the location parameters,

$$\boldsymbol{FIM}_{\boldsymbol{p}_u} = \mathbb{E}(\boldsymbol{D}_{Est}^{\top} \boldsymbol{R}_{Est} \boldsymbol{D}_{Est}) \tag{26}$$

$$\boldsymbol{D}_{Est} = diag\left(\sigma_{d_{RU,1}}^{-2}, \dots, \sigma_{d_{RU,N_{RIS}}}^{-2}, \sigma_{\varphi_{RU,1}}^{-2}, \dots, \sigma_{\varphi_{RU,N_{RIS}}}^{-2}\right) \tag{27}$$

$$\boldsymbol{R}_{Est} = \begin{bmatrix} \frac{x_U - x_{R_1}}{d_{RU,1}} & \frac{y_U - y_{R_1}}{d_{RU,1}} \\ \vdots & \vdots \\ \frac{x_U - x_{R_{N_{RIS}}}}{d_{RU,N_{RIS}}} & \frac{y_U - y_{R_{N_{RIS}}}}{d_{RU,N_{RIS}}} \\ \frac{y_U - y_{R_1}}{s_1^2} & \frac{x_U - x_{R_1}}{s_1^2} \\ \vdots & \vdots \\ \frac{y_U - y_{R_{N_{RIS}}}}{s_{N_{RIS}}^2} & \frac{x_U - x_{R_{N_{RIS}}}}{s_{N_{RIS}}^2} \end{bmatrix} \quad (28)$$

$$s_i = \sqrt{\left(x_U - x_{R_i}\right)^2 + \left(y_U - y_{R_i}\right)^2} \quad \dots\ i \in (1, 2, .., N_{RIS}) \quad (29)$$

4. SIMULATION MODEL AND NUMERICAL RESULTS

4.1. Simulated Scenario

To investigate the model in section 3.1 with different parameters and evaluate the proposed algorithm's performance in section 3.2, we have implemented the simulation scenarios and consider the setup in Fig. 3.

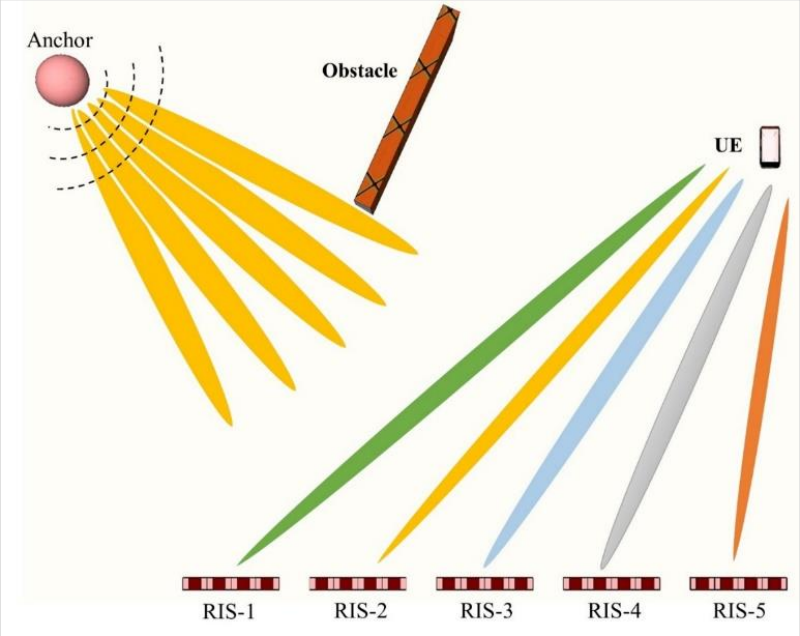

Fig. 3. Simulation Setup.

The parameters are set up as follows: the x-axis points of RIS-1 to RIS-5 are $(-10, -5, 0, 5, 10)$ meters, respectively, while the y-axis points for all the RISs are zeroes, $\boldsymbol{p}_A = (-50, 80)$, the UE is assumed to be uniformly distributed in the working area which is bounded by (10,50) meters and (40,80) meters on x-axis and y-axis respectively.

Regarding the communication and channel parameters, we considered the values that are consistent with the suggested in [19, 20, 28, 31–33]. So, the carrier frequency is equal to $f_c = 28\ GHz$, subcarrier spacing $\Delta_f = 120\ kHz$, OFDM subcarriers and pilot symbols $N_{sc} = 128$ and $T = 256$ is used accurate ToA estimation, IFFT oversampling $N_{os} = 8$, the transmitted power $P_T = 23$ dBm, the noise power spectral density is set to $N_{os} = -170$ dBm/Hz, the path loss exponent $\mu = 2.08$.

4.2. Discussion

4.2.1. Impact of RIS Elements Number on the Location Estimation for Model 1

The simulation results in this section are obtained from model 1 in section 3.1 which use ToA and AoD in a single RIS scenario discussed in [28]. In Fig. 4 the average error of the localization versus the number of RIS elements for various numbers of beams used in the beam sweeping process is illustrated. As depicted in Fig. 4, increasing of the number of beams has a great impact on the localization accuracy for the same number of RIS elements, e.g., when the number of elements is 256, the error decreased from about 3.76 *m* to 21 *cm* using 4 and 64 beams, respectively. On the other hand, the error exhibits flooring when the number of elements exceeds 256 elements for most of the cases particularly when the number of beams is greater than 16.

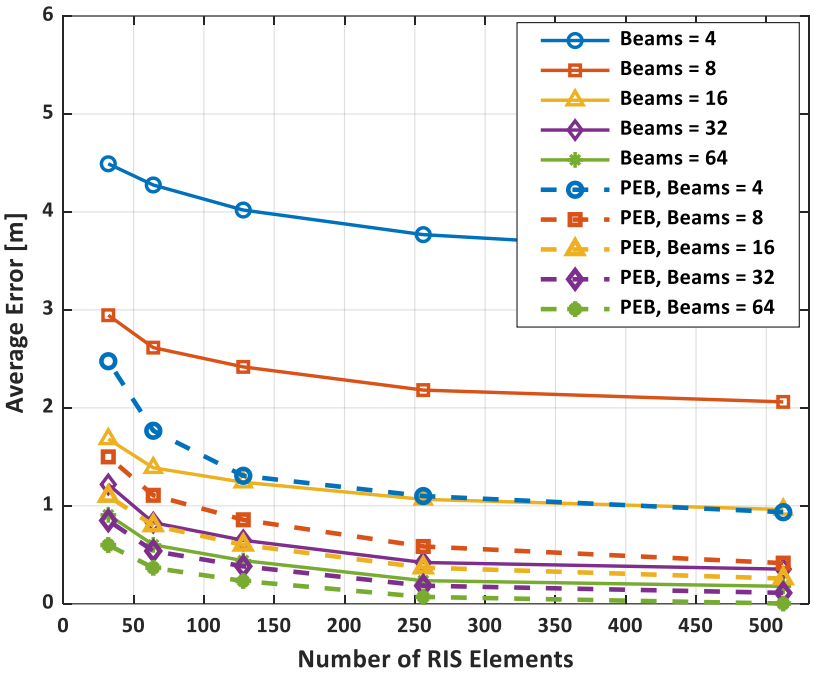

Fig. 4. Average localization error versus number of RIS elements for the single RIS model.

This appears more clearly by plotting the average error versus the number of beams for a different number of RIS elements as illustrated in Fig. 5. Moreover, the numerical results are benchmarked by evaluating PEB for the considered localization parameters which demonstrated that the performance converges the bound when sufficient number of beams is used. It can be concluded that the number of beams significantly affects the localization accuracy as the beams should scan the working area with fine grained resolution.

On the other hand, using RIS with a large number of elements demonstrated a marginal effect on the localization accuracy particularly when plentiful beams are used to scan the region of interest. This motivates to use of multi-RIS that contains a critically sufficient number of RIS elements for the beamforming design.

4.2.2. Impact of Number of RISs and Beams on the Location Estimation for the Proposed Model 2

The simulation results in this section are obtained from model 2 in section 3.2 which uses only AoDs in a multi-RIS scenario, where the AoDs are estimated by exploiting the beam sweeping. All the results in this section use 128 elements in each RIS guided by the simulation

result obtained in Fig. 5. The average localization error for the proposed localization method is evaluated in Fig. 6 for different numbers of RISs versus the number of beams for each RIS. As illustrated, the localization error is significant when using only two RISs, and the error is decreased by increasing the number of RISs.

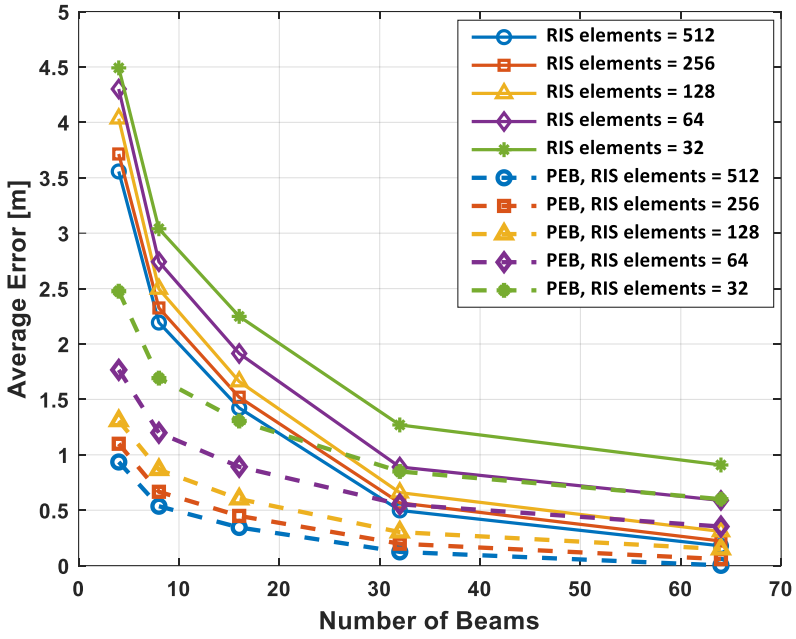

Fig. 5 Average localization error versus number of beams for the single RIS model.

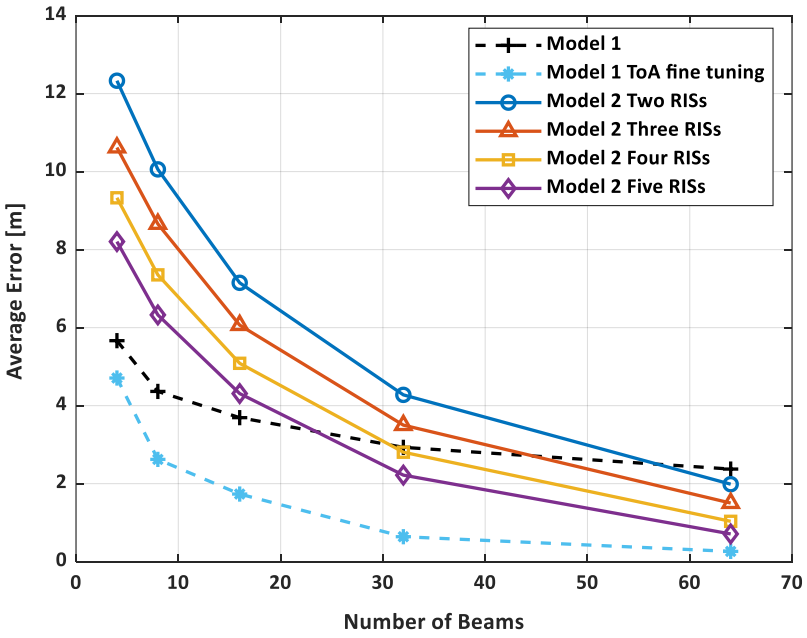

Fig. 6. Average localization error versus number of beams for the proposed multi-RIS model.

The reduction in the error appears brightly using 64 beams for each RIS, as it decreased from 1.96 m to 0.7 m by using two RISs and five RISs respectively. That means that this method needs a sufficient number of beams in addition to enough RISs to provide the diversity of the localization parameters, that is because only the angles (AoDs) are used to estimate the position of the UE and those angles are obtained from choosing the highest received signal corresponding to a known sweeping angle. In addition, the accuracy of the proposed multi-RIS

localization outperforms the performance of the single RIS with ToA estimation by increasing the number of RISs and the number of beams.

Nevertheless, the performance of single RIS with ToA estimation is shown to outperform the localization model 2 presented in this paper when the number of beams is not sufficient to scan the region of interest due to the additional radio measurement provided by ToA that does not rely on beam sweeping. However, the performance of the two models converges when the ToA is fine-tuned using search optimization when the number of beams and RISs is sufficient.

Furthermore, it should be emphasized that the localization procedure of model 2 proposed in this paper alleviates the requirement of ToA estimation used in model 1 which requires significant computational complexity due to the use of IFFT for a sufficient number of transmissions and search optimization to obtain accurate estimation of ToA.

The cumulative distribution functions (CDFs) of the localization errors using 8, 16, 32 and 64 beams are shown in Fig. 7a, b, c, and d, respectively. The CDFs of positioning errors using two, three, four and five RISs are shown in green, blue, red, and black curves respectively. As illustrated in Fig. 7, it is obvious that positioning results improved by increasing the number of beams for the beam sweeping and the number of RISs. Fig. 8 summarizes the CDF evaluation for the cases of using three, four, and five RISs and changing the number of beams from 4 to 64 to sweep the working area.

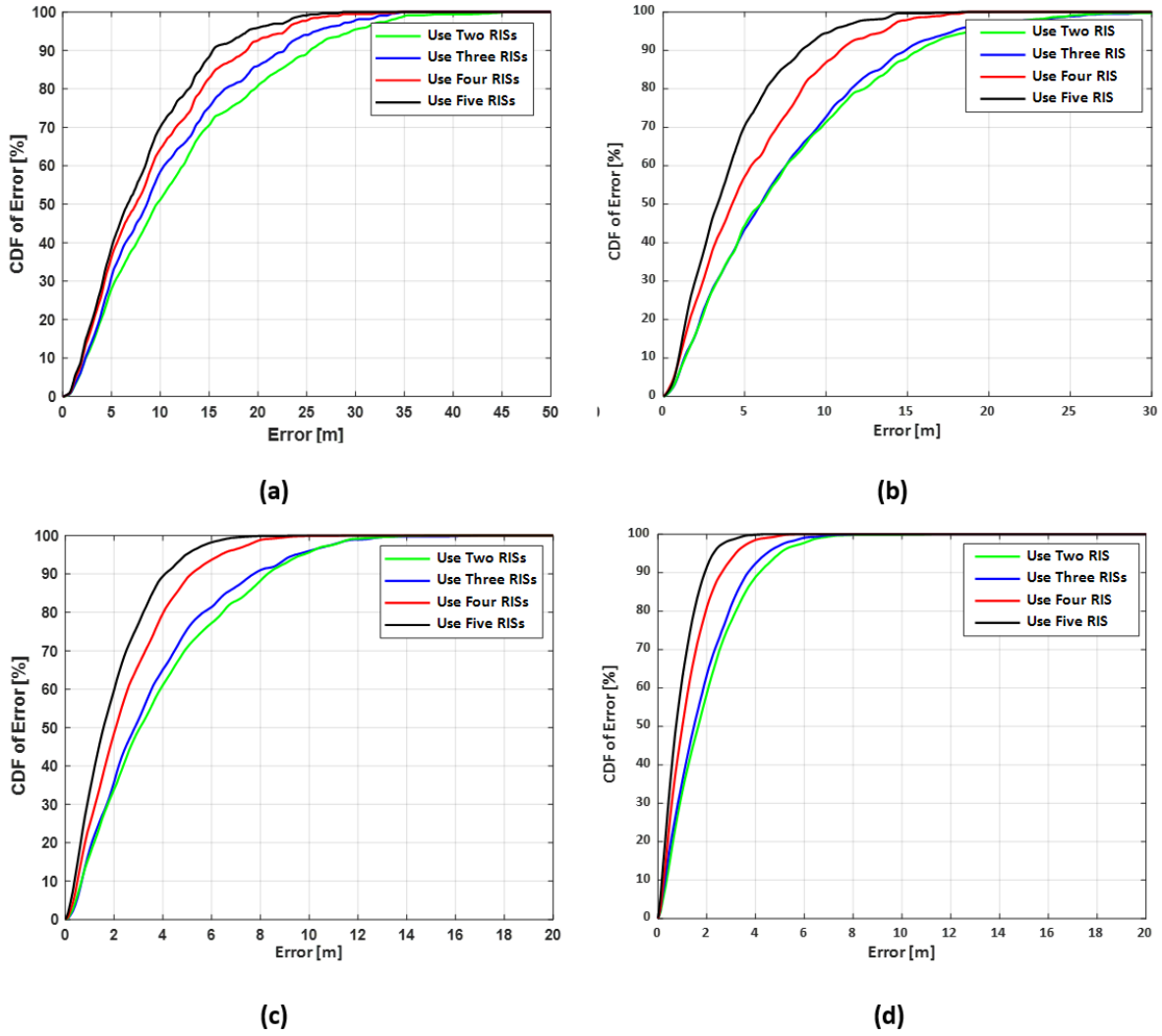

Fig. 7. CDFs of the localization error using AoDs measurements using: a) 8-beams; b) 16-beams; c) 32-beams; d) 64-beams.

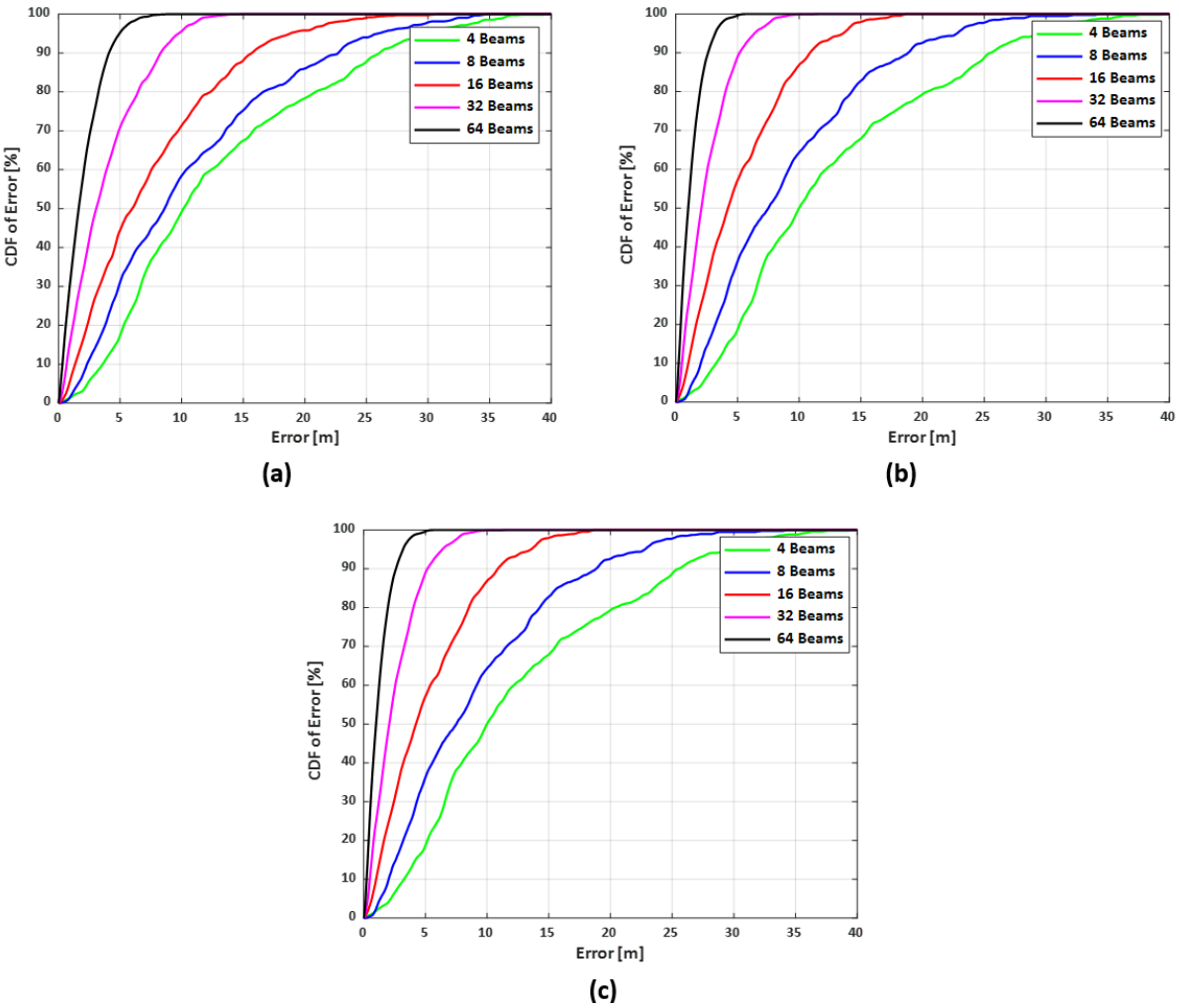

Fig. 8. CDFs of the localization error using AoDs measurements using: a) 3-RISs; b) 4-RISs; c) 5-RISs.

It is essential to highlight the strengths and weaknesses of the proposed scheme then highlight the trade-offs associated with the proposed method to provide a comprehensive and balanced perspective. The proposed scheme shows improved localization accuracy with the adoption of multi-RIS compared to a single RIS using coarse ToA and AoD estimations. In addition, the computational complexity of the proposed method has been alleviated by eliminating the ToA estimation and that will make the system more efficient with respect to energy consumption. On the other hand, multi-RIS scenario need extra transmissions to perform the beam-sweeping process for each RIS towards the area of interest, these additional transmissions can potentially increase the latency and might impose some restrictions in applications that require low-latency responses.

5. CONCLUSIONS

This paper discussed the performance evaluation of RIS aided localization model considering single and multi-RIS scenarios using beam sweeping approach for the region of interest to estimate the AoD. A thorough investigation of the single RIS localization model that adopts both ToA and AoD estimation is presented via numerical simulation and PEB benchmark. It is demonstrated that a sufficient number of beams is required to achieve reasonable localization accuracy while the increase in the number of RIS elements has a marginal impact on the performance. In addition, a localization scheme that adopts multi-RISs

for the estimation of AoDs is proposed in this paper. The intersection of AoD measurements with consensus-based fusion of the estimations is adopted. The proposed scheme alleviates the need for ToA estimation which requires IFFT computation for a sufficient number of transmissions and fine tuning the estimation using computational complex search optimization. The proposed scheme has low computational complexity compared with the single RIS that requires the estimation of ToA while numerical simulation results demonstrated that the proposed scheme provides sufficient and acceptable coarse localization accuracy with the adoption of multi-RISs outperforming the performance of single RIS that employs coarse ToA and AoD estimations. Considering the low computational complexity and sufficient localization accuracy, the proposed scheme requires extra transmissions during beam-sweeping process.

REFERENCES

[1] J. Peral-Rosado, R. Raulefs, J. López-Salcedo, G. Seco-Granados, "Survey of cellular mobile radio localization methods: from 1G to 5G," *IEEE Communications Surveys & Tutorials*, vol. 20, no. 2, pp. 1124–1148, 2018, doi: 10.1109/COMST.2017.2785181.

[2] S. Bartoletti, H. Wymeersch, T. Mach, O. Brunnegard, D. Giustiniano, P. Hammarberg, M. Keskin, J. Lacruz, S. Razavi, J. Rönnblom, F. Tufvesson, J. Widmer, N. Melazzi, "Positioning and sensing for vehicular safety applications in 5G and beyond," *IEEE Communications Magazine*, vol. 59, no. 11, pp. 15–21, 2021, doi: 10.1109/MCOM.011.2100339.

[3] A. Fascista, A. Coluccia, H. Wymeersch, G. Seco-Granados, "Low-complexity accurate mmWave positioning for single-antenna users based on angle-of-departure and adaptive beamforming," IEEE International Conference on Acoustics, Speech and Signal Processing, 2020, doi: 10.1109/ICASSP40776.2020.9053493.

[4] A. Alhafid, S. Younis, "Observed time difference of arrival based position estimation for LTE systems: simulation framework and performance evaluation," *Eastern-European Journal of Enterprise Technologies*, vol. 3, no. 9, pp. 20–28, 2020, doi: 10.15587/1729-4061.2020.201382.

[5] H. Wymeersch, G. Seco-Granados, G. Destino, D. Dardari, F. Tufvesson, "5G mmWave positioning for vehicular networks," *IEEE Wireless Communications*, vol. 24, no. 6, pp. 80–86, 2017, doi: 10.1109/MWC.2017.1600374.

[6] S. Dwivedi, R. Shreevastav, F. Munier, J. Nygren, I. Siomina, Y. Lyazidi, D. Shrestha, G. Lindmark, P. Ernström, E. Stare, S. Razavi, S. Muruganathan, G. Masini, A. Busin, F. Gunnarsson, "Positioning in 5G networks," *IEEE Communications Magazine*, vol. 59, no. 11, pp. 38–44, 2021, doi: 10.1109/MCOM.011.2100091.

[7] A. Fascista, M. Keskin, A. Coluccia, H. Wymeersch, G. Seco-Granados, "RIS-aided joint localization and synchronization with a single-antenna receiver: beamforming design and low-complexity estimation," *IEEE Journal of Selected Topics in Signal Processing*, vol. 16, no. 5, pp. 1141–1156, 2022, doi: 10.1109/JSTSP.2022.3177925.

[8] R. Keating, M. Saily, J. Hulkkonen, J. Karjalainen, "Overview of positioning in 5G new radio," *International Symposium on Wireless Communication Systems*, vol. 2019, pp. 320–324, 2019, doi: 10.1109/ISWCS.2019.8877160.

[9] Y. Ghazaoui, A. ElAlami, M. ElGhzaoui, S. Das, D. Barad, S. Mohapatra, "Millimeter wave antenna with enhanced bandwidth for 5G wireless application," *Journal of Instrumentation*, vol. 15, no. 1, 2020, doi: 10.1088/1748-0221/15/01/T01003.

[10] D. Dardari, "Communicating with large intelligent surfaces: fundamental limits and models," *IEEE Journal on Selected Areas in Communications*, vol. 38, no. 11, pp. 2526–2537, 2020, doi: 10.1109/JSAC.2020.3007036.

[11] B. Ceniklioglu, D. Tubail, A. Canbilen, I. Develi, S. Ikki, "Error analysis of the joint localization and

synchronization of RIS-assisted mm-Wave MISO-OFDM under the effect of hardware impairments," *IEEE Open Journal of the Communications Society*, vol. 3, pp. 2151–2161, 2022, doi: 10.1109/OJCOMS.2022.3203162.

[12] M. Syed, H. Attaullah, S. Ali, M. Aslam, "Wireless communications beyond antennas: the role of reconfigurable intelligent surfaces," *Engineering Proceedings*, vol. 32, no. 1, p. 10, 2023, doi: 10.3390/engproc2023032010.

[13] C. Huang, A. Zappone, G. Alexandropoulos, M. Debbah, C. Yuen, "Reconfigurable intelligent surfaces for energy efficiency in wireless communication," *IEEE Transactions on Wireless Communications*, vol. 18, no. 8, pp. 4157–4170, 2019, doi: 10.1109/TWC.2019.2922609.

[14] Z. Chen, B. Ning, C. Han, Z. Tian, S. Li, "Intelligent reflecting surface assisted terahertz communications toward 6G," *IEEE Wireless Communication*, vol. 28, no. 6, pp. 110–117, 2021, doi: 10.1109/MWC.001.2100215.

[15] Q. Wu, R. Zhang, "Towards smart and reconfigurable environment: intelligent reflecting surface aided wireless network," *IEEE Communication Magazine*, vol. 58, no. 1, pp. 106–112, 2020, doi: 10.1109/MCOM.001.1900107.

[16] C. Huang, G. Alexandropoulos, A. Zappone, M. Debbah, C. Yuen, "Energy efficient multi-user miso communication using low resolution large intelligent surfaces," *IEEE Globecom Workshops*, 2019, doi: 10.1109/GLOCOMW.2018.8644519.

[17] D. Tubail, B. Ceniklioglu, A. Canbilen, I. Develi, S. Ikki, "Error bounds for 3D localization and maximum likelihood estimation of mm-wave MISO OFDM systems in the presence of hardware impairments," *IEEE Communication letter*, vol. 26, no. 9, pp. 2042–2046, 2022, doi: 10.1109/LCOMM.2022.3186789.

[18] E. Bjornson, H. Wymeersch, B. Matthiesen, P. Popovski, L. Sanguinetti, E. Carvalho, "Reconfigurable intelligent surfaces: a signal processing perspective with wireless applications," *IEEE Signal Processing Magazine*, vol. 39, no. 2, pp. 135–158, 2022, doi: 10.1109/MSP.2021.3130549.

[19] K. Keykhosravi, M. Keskin, G. Seco-Granados, H. Wymeersch, "SISO RIS-enabled joint 3D downlink localization and synchronization," IEEE International Conference on Communications, 2021, doi: 10.1109/ICC42927.2021.9500281.

[20] A. Al-Hourani, S. Chandrasekharan, S. Kandeepan, "Path loss study for millimeter wave device-to-device communications in urban environment," IEEE International Conference on Communications, 2014, doi: 10.1109/ICCW.2014.6881180.

[21] A. Alhafid, S. Younis, Y. Ali, "Efficient near-field localization aided with reconfigurable intelligent surface using geometric dilution of precision," *Journal of Information and Telecommunication*, vol. 4, no. 7, pp. 1–23, 2023, doi: 10.1080/24751839.2023.2272488.

[22] D. Dardari, N. Decarli, A. Guerra, F. Guidi, "LOS/NLOS near-field localization with a large reconfigurable intelligent surface," *IEEE Transactions on Wireless Communications*, vol. 21, no. 6, pp. 4282–4294, 2022, doi: 10.1109/TWC.2021.3128415.

[23] A. Kh, S. Younis, Y. Ali, "Efficient near-field localization aided with reconfigurable intelligent surface using geometric dilution of precision efficient near-field localization aided with reconfigurable intelligent surface using geometric dilution of precision," *Journal of Information and Telecommunication*, vol. 7, no. 4, pp. 1–23, 2023, doi: 10.1080/24751839.2023.2272488.

[24] A. Alhafid, Y. Ali, S. Younis, "Performance investigation of RIS aided localization with TDoA in the near-field," *Mathematical Modelling of Engineering Problems*, vol. 10, no. 6, pp. 2127–2134, 2023, doi: 10.18280/mmep.100624.

[25] T. Wu, C. Pan, Y. Pan, S. Hong, H. Ren, M. Elkashlan, "Two-step mmWave positioning scheme with RIS-part I : angle estimation and analysis," *arXiv - EE - Signal Processing*, vol. 8, pp. 1–30, 2022, doi: 10.48550/arXiv.2208.07602.

[26] G. Alexandropoulos, I. Vinieratou, H. Wymeersch, "Localization via multiple reconfigurable intelligent surfaces equipped with single receive RF chains," *IEEE Wireless Communication Letter*,

vol. 11, no. 5, pp. 1072–1076, 2022, doi: 10.1109/LWC.2022.3156427.

[27] G. Seco-granados, S. Member, H. Wymeersch, S. Member, "Joint user localization and location calibration of a hybrid reconfigurable intelligent surface," *arXiv - EE - Signal Processing,* vol. 10, pp. 1–5, 2022, doi: 10.48550/arXiv.2210.10150

[28] M. Ammous, S. Valaee, "Cooperative positioning with the aid of reconfigurable intelligent surfaces and device-to-device communications in mmWave," 33rd Annual International Symposium on Personal, Indoor and Mobile Radio Communications, 2022, doi: 10.1109/PIMRC54779.2022.9977483.

[29] D. Emenonye, H. Dhillon, R. Buehrer, "Fundamentals of RIS-aided localization in the far-field," *arXiv - EE - Signal Processing*, vol. 6, 2022, doi: 10.48550/arXiv.2206.01652.

[30] Q. Wu, S. Zhang, B. Zheng, C. You, R. Zhang, "Intelligent reflecting surface-aided wireless communications: a tutorial," *IEEE Transactions on Communications*, vol. 69, no. 5, pp. 3313–3351, 2021, doi: 10.1109/TCOMM.2021.3051897.

[31] J. He, H. Wymeersch, T. Sanguanpuak, O. Silven, M. Juntti, "Adaptive beamforming design for mmWave RIS-Aided joint localization and communication," IEEE Wireless Communications and Networking Conference Workshops, 2020, doi: 10.1109/WCNCW48565.2020.9124848.

[32] J. He, H. Wymeersch, L. Kong, O. Silven, M. Juntti, "Large intelligent surface for positioning in millimeter wave MIMO systems," IEEE 91st Vehicular Technology Conference, 2020, doi: 10.1109/VTC2020-Spring48590.2020.9129075.

[33] Q. Wu, R. Zhang, "Beamforming optimization for wireless network aided by intelligent reflecting surface with discrete phase shifts," *IEEE Transactions on Communications*, vol. 68, no. 3, pp. 1838–1851, 2020, doi: 10.1109/TCOMM.2019.2958916.

[34] X. Yuan, Y. Zhang, Y. Shi, W. Yan, H. Liu, "Reconfigurable-intelligent-surface empowered wireless communications: challenges and opportunities," *IEEE Wireless Communications*, vol. 28, no. 2, pp. 136–143, 2021, doi: 10.1109/MWC.001.2000256.

[35] M. Win, Z. Wang, Z. Liu, Y. Shen, A. Conti, "Location awareness via intelligent surfaces: a path toward holographic NLN," *IEEE Vehicular Technology Magazine*, vol. 17, no. 2, pp. 37–45, 2022, doi: 10.1109/MVT.2022.3157067.

[36] L. Tran, A. Le, X. Huang, E. Dutkiewicz, D. Ngo, A. Taparugssanagorn, "Complexity reduction for hybrid TOA/AOA localization in UAV-assisted WSNs," *IEEE Sensors Letters*, vol. 7, no. 11, p. 7005904, 2023, doi: 10.1109/LSENS.2023.3322968.

[37] D. Dardari, N. Decarli, A. Guerra, F. Guidi, "LOS/NLOS near-field localization with a large reconfigurable intelligent surface," *IEEE Transactions on Wireless Communications*, vol. 21, no. 6, pp. 4282–4294, 2022, doi: 10.1109/TWC.2021.3128415.

[38] A. Elzanaty, A. Guerra, F. Guidi, M. Alouini, "Reconfigurable intelligent surfaces for localization: position and orientation error bounds," *IEEE Transactions on Signal Processing*, vol. 69, pp. 5386–5402, 2021, doi: 10.1109/TSP.2021.3101644.